DUCTILE FRACTURE STRAIN IN UNIAXIAL TENSILE TEST OF PLANE SPECIMEN'S

MOHAMED ZULQARNAIN BIN MOHAMED AKRAM

Report submitted in partial fulfillment of the requirements
for the award of the degree of Bachelor of Mechanical Engineering

Faculty of Mechanical Engineering
UNIVERSITI MALAYSIA PAHANG

JUNE 2012

ABSTRACT

This project was performed to determine the ductile fracture strain in uniaxial tensile test of plane specimen. In this project, uniaxial tensile test was performed for three difference material that is aluminum, brass and mild steel. The objective of the test is to identify the value of uniaxial fracture strain for these three difference materials. The specimens have been divided into three difference area: L, P-lateral and S-middle zones. The zones are measured using optical microscope before and after the tensile test to determine the value of ductile fracture strain at those zones. However, the result from tensile test gives an average value of ductile fracture strain. The second step was to determine the suitable point or area to get the accurate uniaxial ductile fracture strain. The element of the material with stress triaxiality,k = 0.33 is the location where the uniaxial fracture strain was occurred. Finite element analysis using MSC Patran/Marc 2008r1 software was used to determine the element with stress triaxiality,k = 0.33. In MSC Patran software, the specimen was divided into several nodes to represent the study location for lateral and middle zones. In this project, the model was divided into eleven points. Each point has differences values of stress triaxiality after ultimate tensile strength occurred. The finite element analysis data of engineering stress-strain curve was compared with experiment engineering stress-strain curve in order to determine the fracture point of the model. The state of stress for each material was determined in order to get the uniaxial ductile fracture strain nodes. The result shows that uniaxial ductile fracture strain occurred at nodes 2577 for aluminium and brass, while uniaxial ductile fracture strain for mild steel occurred at node 2598. It is also shown that the fracture strain at L and P-lateral zones was the nearest to the uniaxial ductile fracture strain.

ABSTRAK

Projek ini telah dijalankan untuk menentukan terikan patah mulur dalam ujian tegangan ekapaksi spesimen satah. Dalam projek ini, ujian tegangan sepaksi telah dilakukan untuk tiga bahan yang berbeza iaitu aluminium, tembaga dan keluli lembut. Objektif ujian ini adalah untuk mengenal pasti nilai terikan patah unipaksi untuk ketiga-tiga bahan berbeza. Spesimen telah dibahagikan kepada tiga kawasan berbeza: L, P-sisi dan zon S-tengah. Zon diukur dengan menggunakan mikroskop optik sebelum dan selepas ujian tegangan untuk menentukan nilai terikan patah mulur di zon-zon berkenaan. Walau bagaimanapun, hasil daripada ujian tegangan memberikan nilai purata terikan patah mulur. Langkah kedua adalah untuk menentukan titik atau kawasan yang sesuai untuk mendapatkan nilai patah yang tepat berketegangan mulur ekapaksi. Unsur bahan dengan triaxiality tegasan, k = 0.33 adalah lokasi di mana terikan patah ekapaksi telah berlaku. Analisis unsur terhingga menggunakan perisian MSC Patran / Marc 2008r telah digunakan untuk menentukan elemen dengan triaxiality tegasan, k = 0.33. Dalam perisian MSC Patran, spesimen telah dibahagikan kepada beberapa nod mewakili lokasi kajian untuk zon sisi dan sederhana. Dalam projek ini, model itu dibahagikan kepada 11 titik. Setiap titik mempunyai perbezaan nilai triaxiality tegasan selepas kekuatan tegangan muktamad berlaku. Analisis terhingga data unsur lengkung kejuruteraan tegasan-terikan berbanding dengan eksperimen kejuruteraan lengkung tegasan-terikan untuk menentukan titik patah model. Keadaan tegasan bagi setiap bahan yang telah ditentukan untuk mendapatkan terikan ekapaksi nod patah mulur. Hasilnya menunjukkan bahawa ketegangan patah mulur ekapaksi yang berlaku pada nod 2577 untuk aluminium dan tembaga, manakala terikan patah mulur ekapaksi untuk keluli lembut berlaku pada nod 2598. Ia juga menunjukkan bahawa terikan patah di zon L dan P hala adalah yang terdekat untuk terikan patah mulur ekapaksi.

TABLE OF CONTENTS

		Page
SUPERVISOR'S DECLARATION		ii
STUDENT'S DECLARATION		iii
DEDICATION		iv
ACKNOWLEDGEMENT		v
ABSTRACT		vi
ABSTRAK		vii
TABLE OF CONTENTS		viii
LIST OF TABLES		xi
LIST OF FIGURES		xii
LIST OF SYMBOLS		xvi
LIST OF ABBREVIATIONS		xvii
CHAPTER 1	**INTRODUCTION**	
1.1	Research Background	1
1.2	Problem Statement	2
1.3	Objectives	3
1.4	Scopes Of Study	3
CHAPTER 2	**LITERATURE REVIEW**	
2.1	Introduction	4
2.2	Experimental Test Setup	4
2.3	Wire-Cut EDM Review	7
2.4	Engineering Stress-Strain Curve	8
2.5	True Stress-Strain Curve	11

2.6 Finite Element Analysis (FEA) Simulation 15

2.7 Stress Triaxiality And Ductile Fracture Strain 19

CHAPTER 3 METHODOLOGY

3.1 Introduction 23

3.2 Research Flow Chart 23

3.3 Specimen Preparation 25

3.3.1 Specimen Specification 25
3.3.2 Machining Process 26
3.3.3 Polishing Process 30
3.3.4 Zone Marking Process 31

3.4 Tensile Test 34

3.5 Measurement Of Zone Length 37

3.6 Finite Element Analysis (FEA) 39

3.6.1 Modeling, Meshing and Solving Process 40

CHAPTER 4 RESULT AND DISCUSSION

4.1 Introduction 52

4.2 Experiment Result 52

4.2.1 Engineering Stress-Strain Graph 53
4.2.2 Conversion of Engineering Stress-Strain Curve To True Stress-Strain Curve 56
4.2.3 The Result For Every Zone 60

4.3 Finite Element Analysis (FEA) Result 64

4.4 Ductile Fracture Strain 73

4.5 Stress Triaxiality 78

CHAPTER 5 CONCLUSION AND RECOMMENDATION

5.1 Conclusion 85
5.2 Recommendation 86

REFERENCES 87

APPENDICES

Appendix A 89
Appendix B 90
Appendix C 91
Appendix D 92
Appendix E 93
Appendix F 94

LIST OF TABLES

Table No.		Page
2.1	Chemical composition of BV-DH32 steel	6
2.2	Typical mechanical properties of BV-DH32 steel	6
2.3	Breadth and thickness in reduced section	6
2.4	Measured mechanical properties of BV Grade DH32 steel	20
2.5	Comparison of equivalent strain to fracture of dog-bone specimen between simulations and test of dog-bone specimens	21
3.1	The direction of polishing process for difference sandpaper grit number	30
3.2	The value of young modulus and poison ratio for each material used	45
4.1	Mechanical properties of Aluminum obtained from tensile test	54
4.2	Mechanical properties of Brass obtained from tensile test	55
4.3	Mechanical properties of Mild steel obtained from tensile test	56
4.4	Mechanical properties of material tested	59
4.5	Experimental result for ductile fracture strain	62
4.6	Specimen’s geometry and average strain values in analyzed regions	63
4.7	The stress triaxiality at every node for aluminum specimen	79
4.8	The stress triaxiality at every node for brass specimen	81
4.9	The stress triaxiality at every node for mild steel specimen	82
4.10	Ductile fracture strain for aluminum at different zones	84
4.11	Ductile fracture strain for brass at different zones	84
4.12	Ductile fracture strain for mild steel at different zones	84

LIST OF FIGURES

Figure No.		Page
1.1	Cross-sectional area in the neck at fracture: a) before fracture, and b) after fracture	2
2.1	A photo of test set up for specimen P34	7
2.2	Engineering stress strain curve for a typical engineering alloy	9
2.3	Comparison of engineering and true stress-strain curves	10
2.4	Typical stress-strain curve	12
2.5	Example of true stress-strain plot	14
2.6	Stress triaxiality,*k* for an individual plane stress cases: a) biaxial compression, b) uniaxial compression, c) simple shear d) uniaxial tension e) biaxial tension	17
2.7	Comparison of stress triaxiality in different specimen zone: L, P – lateral, S – middle	17
2.8	Shape of plane specimen at fracture point obtained from Finite Element Analysis (FEA)	18
2.9	The moving grids in local necking zone: a) ε_p =0.41, and b) ε_p =1.42 (close to fracture	19
2.10	The evolution of stress triaxiality calculated by ADINA	22
3.1	Research flow chart	24
3.2	The standard ASTM tensile test dimension for plane specimen	26
3.3	The wire use to cut the material in wire cut machine	27
3.4	Wire cut machine: a) water is use as dielectric liquid, b) wire rotating area	28
3.5	The software use to generate wire cut machine	29
3.6	The straight line from wire cut drawing for first step of cutting the specimen	29

3.7	The second step of drawing that use in cutting material to get tensile specimen	30
3.8	The surface finish after polishing using sandpaper	31
3.9	The highlight region at gauge length	32
3.10	The marking zone with three zone: a) lateral-zone L and P, b) middle-zone S	33
3.11	The marking zone for aluminum specimen	33
3.12	Example of marking zone at tensile specimen	34
3.13	The specimen condition after break for aluminum	35
3.14	The specimen condition after break for brass	35
3.15	The specimen condition after break for mild steel	36
3.16	The specimen break during tensile test	36
3.17	The position of specimen when using microscope	37
3.18	The position of dial gauge when during measurement	38
3.19	The measurement process by using microscope and dial gauge	38
3.20	Distribution of stress triaxiality k: a) Initial phase of tensile test, and b) Final phase of tensile test	40
3.21	Step in PATRAN software	41
3.22	The setting for create a point coordinate	41
3.23	The step in GEOMETRY part from: a) point coordinate, b) make line to combine the point, c) make surface, d) change surface direction	42
3.24	The solid part of the specimen in quarter shape	42
3.25	Step for ELEMENT part: a) mesh seed process, b) the meshing process and c) equivalence process	43
3.26	Step to create boundary condition at the specimen	44
3.27	The FIELD part input data	44
3.28	The PROPERTIES part to change the option into reduced integration	46
3.29	Input properties part	46

3.30	Input data for application region	47
3.31	The analysis part in PATRAN software	48
3.32	The step in job parameter part	48
3.33	Step in load step creation part to set the load increment parameter	49
3.34	Step in load step creation part to set the iteration parameter	49
3.35	The step for load step selection	50
3.36	The step to read the result	50
4.1	Stress versus strain curve for aluminum	53
4.2	Stress versus strain curve for brass	54
4.3	Stress versus strain curve for mild steel	55
4.4	True plastic stress-strain curve for aluminum	57
4.5	True plastic stress-strain curve for brass	58
4.6	True plastic stress-strain curve for mild steel	58
4.7	Failed specimen for all material. From left are aluminum, mild steel and brass	60
4.8	Typical tensile specimen for flat specimen	61
4.9	The elongation of aluminum in finite element analysis	64
4.10	The simulation result for aluminum in 3D view	65
4.11	The shape of saddle at the break point for aluminum	67
4.12	The elongation of brass in finite element analysis	67
4.13	The simulation result for brass in 3D view	67
4.14	The shape of saddle at the break point for brass	68
4.15	The elongation of mild steel in finite element analysis	69
4.16	The simulation result for mild steel in 3D view	70
4.17	The shape of saddle at the break point for mild steel	70
4.18	The comparison of engineering stress-strain data obtained from finite element analysis for different materials	72
4.19	Comparison of stress-strain curve between experiment data and finite element result for aluminum	74

4.20	Comparison of stress-strain curve between experiment data and finite element result for brass	75
4.21	Comparison of stress-strain curve between experiment data and finite element result for mild steel.	76
4.22	Study nodes location in Finite Element Analysis (FEA)	77
4.23	The comparison of stress triaxiality for aluminum in different zones: *L*, *P*-lateral, *S*-middle and all study nodes	78
4.24	The comparison of stress triaxiality for brass in different zones: *L*, *P*-lateral, *S*-middle and all study nodes	80
4.25	The comparison of stress triaxiality for mild steel in different zones: *L*, *P*-lateral, *S*-middle and all study nodes	81

LIST OF SYMBOLS

k	Stress triaxiality
b_0	Breadth length
t_0	Thickness length
σ	Stress, MPa
ε	Strain
$\sigma_{uts} = \sigma_u$	Ultimate tensile strength, MPa
$\sigma_{0.2\%YS} = \sigma_y$	0.2% offset yield strength, MPa
E	Young modulus
A_0	Cross-sectional area
L_0	Length
P	Pressure
ΔL	Total length
K	Strain hardening coefficient
n	Strain hardening exponent
σ_m	Mean normal stress, MPa
σ_H	Equivalent stress, MPa
$\varepsilon_p = \varepsilon_f$	Fracture strain
b_0	Width of specimen before test
b_1	Width of specimen after test
g_0	Length of specimen before test
g_1	Length of specimen after test
$\varepsilon_1 = \varepsilon_2 = \varepsilon_p$	Plastic strain
F	Force, N
σ_E	Engineering stress
σ_T	True stress
ε_E	Engineering strain
ε_T	True strain

LIST OF ABBREVIATIONS

FEA	Finite Element Analysis
ASTM	American Society for Testing and Materials
UTM	Universal Testing Machine
WEDM	Wire-Cut Electrical Discharge Machining
HSTR	High Strength and Temperature Resistive
EDM	Electrical Discharge Machining
FEM	Finite Element Method
CSV	Comma-Separated Values
BC	Boundary Condition
CAD	Computer Aided Design

CHAPTER 1

INTRODUCTION

1.1 RESEARCH BACKGROUND

Uniaxial fracture strain gathered from tensile test for plane specimen are not accurate because the result was calculated based on the average of entire critical cross-section of the specimen. Previous researches show that the fracture strain of plane specimens is not identical across the cross-section.

As reported by most of researchers, the failed plane specimen (after tensile test) shows a shape of saddle as shown in Figure 1.1. Final cross-section of plane specimen is totally changes against its original shape. Therefore, the equation to determine the stress and strain subjected to the specimen (force divided by area) is no longer accurate. In this study the true uniaxial ductile fracture strain of plane specimen will be investigated.

The study was focusing on three different materials which are carbon steel, aluminum and brass. The tensile test has been performed on all material studies to determine the engineering stress-strain curve. The curve obtained from the test then was converted to true engineering stress-strain curve. Then, true plastic stress-strain data was determined to be employed in Finite Element Analysis. In order to determine the uniaxial fracture strain, tensile test will be simulated in Finite Element software.

For this purpose, MSC Patran/Marc 2008r1 was applied. The engineering stress-strain curve from the Finite Element Analysis will be combined with experimental data in order to determine the fracture initiation point. The state of stress for each element in critical cross-section at fracture point then was investigated to determine the uniaxial fracture strain. Finally the result from the experiment has been compared with Finite Element results.

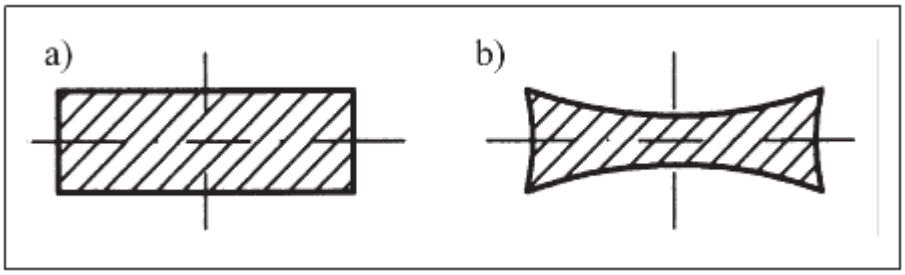

Figure 1.1: Cross-sectional area in the neck at fracture: a) before fracture, b) after fracture

Source: Kut, 2010

1.2 PROBLEM STATEMENT

Design is one of the important process in developing the engineering structure. During design stage, few processes were involved such as analysis of deflection, stress analysis, cost reliability and others. Stress analysis appears as a crucial process as many engineering structure fail due to lack of consideration on this analysis. One of the important parameters involve in stress analysis is uniaxial fracture strain. The failure on engineering structure normally predicted based on maximum stress or strain that can be withstand by the structure. Therefore, the fracture strain becomes crucial to be determined.

As discussed in previous section, the fracture strain can be determined by conducting the uniaxial tensile test. However, as reported by many researchers, the uniaxial fracture strain is very difficult to determined using plane specimens. It is due to the obvious changes in cross-section of plane specimen after tensile test was performed. Many researchers had tried to develop a simple method to calculate or determine the uniaxial fracture strain of the materials. However, there is no reliable method was reported recently.

1.3 OBJECTIVES

The objectives of the research are as follow:

1) To determine the uniaxial ductile fracture strain during tensile test of plane specimen
2) To investigate the state of stress of plane specimen during uniaxial tensile test.

1.4 SCOPES OF STUDY

The scopes of the research are as follow:

1) Specimen preparation
2) Materials used were carbon steel, brass and aluminum.
3) Plane specimen with rectangular cross-section
4) Uniaxial tensile test – at room temperature and refer to ASTM E8 2008
5) Finite Element Analysis (FEA)
    - MSC Patran/Marc
    - Non-linear
    - Large displacement
    - Homogeneous material and model
6) Validation – compare experiment data with finite element analysis result

CHAPTER 2

LITERATURE REVIEW

2.1 INTRODUCTION

This chapter will provide the detail description literature review done according to title of ductile fracture strain in uniaxial tensile test of plane specimen. Literature regarding any development or experiment about fracture strain and state of stress is useful in this project. This is includes the experiment setup, engineering and true stress-strain curve, and finite element analysis software available for analysis.

2.2 EXPERIMENTAL TEST SETUP

The uniaxial tension test is widely used to provide basic information on the mechanical behavior of materials and as an acceptance test for the specification of materials. In this test, a specimen is subjected to a continually increasing uniaxial tensile force while simultaneous observations are made of the extension of the specimen. Load–extension curves are used to construct stress–strain curves, which can provide more useful information on mechanical properties of materials. The most common properties derived from such curves are yield and ultimate strength values, elongation, and reduction of area (Mahmudi, Mohammadi and Sepehrband, 2004).

Flat specimens are machined from thermo mechanically rolled steel plate BV-DH32 with 36 mm thickness. This grade of steel is almost exclusively utilized in shipbuilding for the construction of structural parts of ships and offshore platforms. From mill sheets for the mother plate, the chemical compositions are shown in Table 2.1. Typical mechanical properties at room temperature are summarized in Table 2.2 where the values in parentheses are from mill sheets for the mother plate. As for parallel direction to rolling, three pairs of smooth flat specimens (P33, P34 and P35) are prepared so as to have different aspect ratios by changing thicknesses.

Actual dimensions at the reduced section are listed in Table 2.3. The experiments are conducted with a 300 kN UTM with controlled displacement. With a gauge length of 50 mm, a constant loading speed of 1 mm/min is applied. The loading is stopped every 1mm or 2 mm extension of gauge length to measure the actual thickness and breadth changes at the minimum cross section. Thickness and breadth are manually measured, with digital calipers and micrometer, at the six longitudinally different points to search the minimum cross section even before the onset of necking.

After the onset of necking, six points at the smallest cross section are measured for every increment due to the cushioning effect of specimens with rectangular cross section. Square grids are stenciled on the surface of the breadth side of the specimen to analyze digital images recorded during every test increment same as shown in Figure 2.1. Digital images are taken with a digital camera with a resolution of 2816×2112 pixels. The camera is mounted on a digital height gage to keep consistent barrelling distortion due to lens convexity during elongation of the specimen (Choung and Cho, 2008).

Table 2.1: Chemical composition of BV-DH32 steel

C	Si	Mn	P	S	Cu	Ni	Cr	Mo
0.14	0.28	1.06	0.012	0.003	0.03	0.02	0.03	0.01

Source: Choung and Cho, 2008

Table 2.2: Typical mechanical properties of BV-DH32 steel

Minimum yield strength	Minimum tensile strength	Minimum elongation
315 (355) MPa	440 (480) MPa	22(31) %

Source: Choung and Cho, 2008

Table 2.3: Breadth and thickness in reduced section

No.	b_0	t_0	b_0/t_0
P33	12.044	12.523	0.962
P34	12.030	9.000	1.337
P35	11.950	4.974	2.402

Source: Choung and Cho, 2008

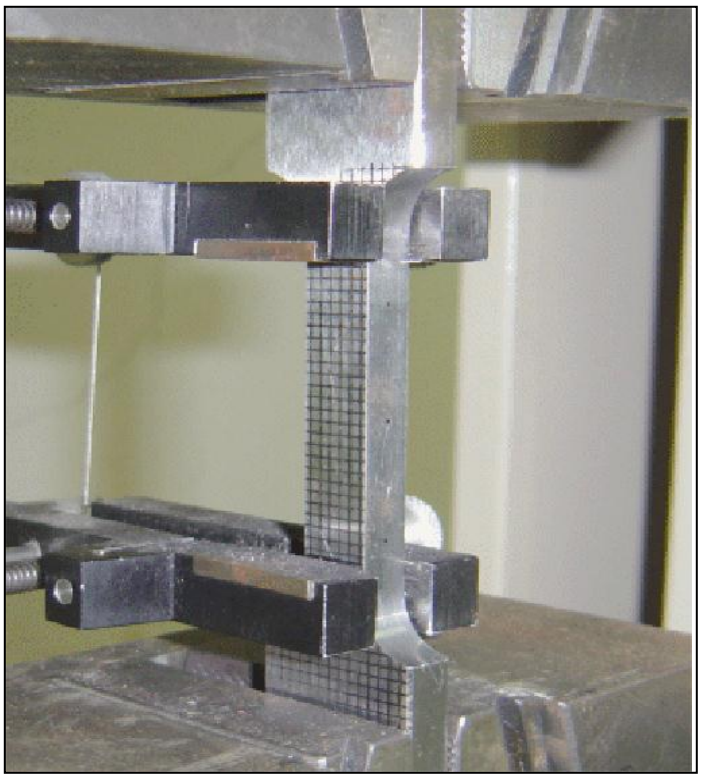

Figure 2.1: A photo of test set up for specimen P34

Source: Choung and Cho, 2008

2.3 WIRE-CUT EDM REVIEW

Wire-cut electrical discharge machining (WEDM) technology has grown tremendously since it was first applied more than 30 years ago. Its broad capabilities have allowed it to encompass the production, aerospace and automotive industries and virtually all areas of conductive material machining. This is because wire EDM provides the best alternative or sometimes the only alternative for machining conductive, exotic and high strength and temperature resistive (HSTR) materials with the scope of generating intricate shapes and profiles. It has proved to have tremendous potential in its applicability in the present day metal cutting industry for achieving a considerable dimensional accuracy, surface finish and contour generation features of products or parts.

WEDM is a thermo-electrical process in which material is eroded from the workpiece by a series of discrete sparks between the workpiece and the wire electrode (tool) separated by a thin film of dielectric fluid (deionised water) which is continuously forced fed to the machining zone to flush away the eroded particles. The movement of the wire is controlled numerically to achieve the desired three-dimensional shape and accuracy for the workpiece. Although, the average cutting speed, relative machining costs, accuracy and surface finish have been improved several times better since the commercial inception of the machine, further improvement is still required to meet the increasing demand of precision and accuracy by different industries.

However, so far precision and accuracy are concerned; the vibrational behaviour and the static deflection of the wire (wire lag) need to be studied simultaneously. Although a good number of researches have been carried out to study the wire lag and its measurement, a very little study has been done over the vibrational behavior of the wire due to numerous complexities.

The complexities arise out in modeling the wire-tool vibration phenomenon, in the solution approach of the vibration equation and also in conducting the experiments for the purpose of measuring the amplitude of the vibration. This originates the necessity to investigate into the vibrational behaviour of the wire in detail as the same plays a major role to decide the precision and accuracy of an electro-discharge machined job (Puri and Bhattacharyya, 2003).

2.4 ENGINEERING STRESS-STRAIN CURVE

The engineering tension test is widely used to provide basic design information on the strength of materials and as an acceptance test for the specification of materials. In the tension test a specimen is subjected to a continually increasing uniaxial tensile force while simultaneous observations are made of the elongation of the specimen.

The shape and magnitude of the stress-strain curve of a metal will depend on its composition, heat treatment, prior history of plastic deformation, and the strain rate, temperature, and state of stress imposed during the testing. The parameters, which are used to describe the stress-strain curve of a metal, are the tensile strength, yield strength or yield point, percent elongation, and reduction of area. The first two are strength parameters; the last two indicate ductility.

An example of the engineering stress-strain curve for a typical engineering alloy is shown in Figure 2.2. From it some very important properties can be determined. The elastic modulus, the yield strength, the ultimate tensile strength, and the fracture strain are all clearly exhibited in an accurately constructed stress strain curve.

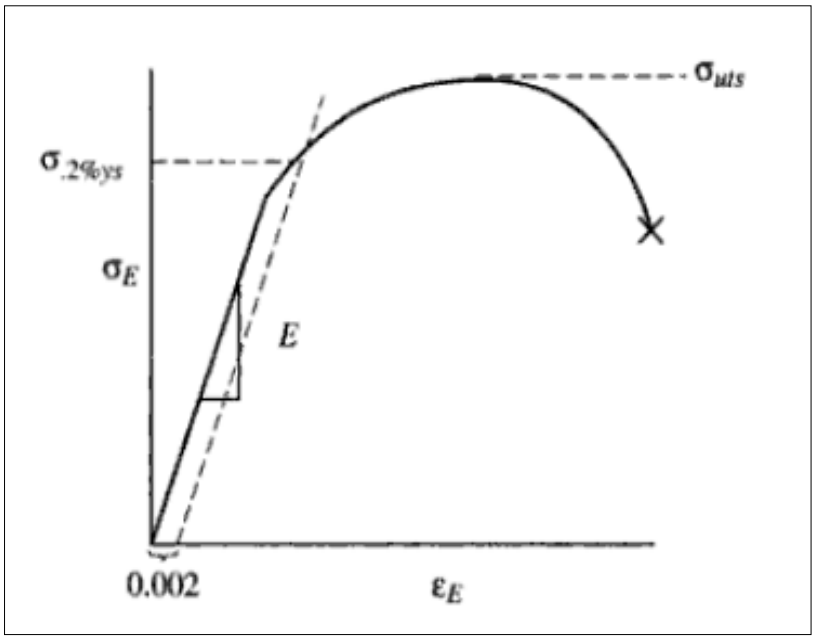

Figure 2.2: Engineering stress strain curve for a typical engineering alloy

The elastic modulus, E (Young's modulus) is the slope of the elastic portion of the curve (the steep, linear region) because E is the proportionality constant relating stress and strain during elastic deformation: $\sigma = E\varepsilon$. The 0.2% offset yield strength is the stress value, $\sigma_{0.2\%YS}$ of the intersection of a line (called the offset) constructed parallel to the elastic portion of the curve but offset to the right by a strain of 0.002. It represents the onset of plastic deformation.

The ultimate tensile strength is the engineering stress value or σ_{uts}, at the maximum of the engineering stress-strain curve. It represents the maximum load, for that original area, that the sample can sustain without undergoing the instability of necking, which will lead inexorably to fracture. The fracture strain is the engineering strain value at which fracture occurred.

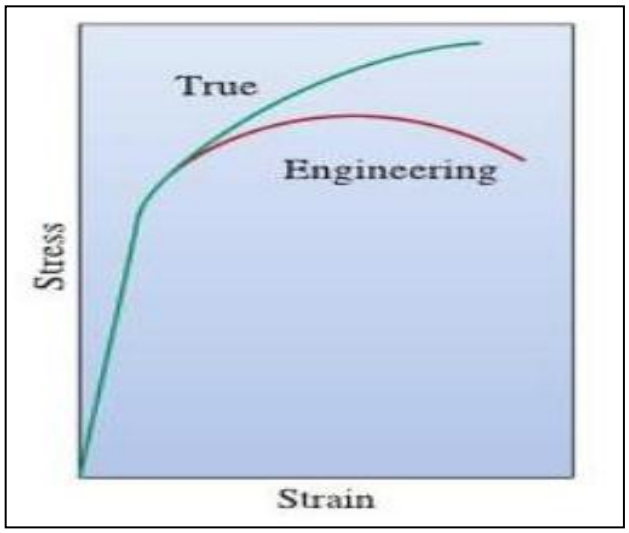

Figure 2.3: Comparison of engineering and true stress-strain curves

The engineering stress is the load borne by the sample divided by a constant, the original area. The true stress is the load borne by the sample divided by a variable the instantaneous area. Note that the true stress always rises in the plastic, whereas the engineering stress rises and then falls after going through a maximum.

The maximum represents a significant difference between the engineering stress-strain curve and the true stress-strain curve. Figure 2.3 show the comparison of engineering and true stress-strain curves. In the engineering stress-strain curve, this point indicates the beginning of necking. The ultimate tensile strength is the maximum load measured in the tension test divided by the original area. The engineering measures of stress and strain denoted in this module as σ_e and ε_e respectively, are determined from the measured the load and deflection using the original specimen cross-sectional area A_0 and length L_0 as equation (2.1) and (2.2):

$$\sigma_e = \frac{P}{A_0} \tag{2.1}$$

$$\varepsilon_e = \frac{\Delta L}{L_0} \tag{2.2}$$

2.5 TRUE STRESS-STRAIN CURVE

During stress testing of a material sample, the stress–strain curve is a graphical representation of the relationship between stress, obtained from measuring the load applied on the sample, and strain, derived from measuring the deformation of the sample. The nature of the curve varies from material to material.